Ghimire, Bidur; Nakashima, Shinichiro; Hosoda, Takashi

Study of Various Flow Regimes in the Water Intrusion Process into Porous Media under Different Upstream Boundary Conditions

STUDY OF VARIOUS FLOW REGIMES IN THE WATER INTRUSION PROCESS INTO POROUS MEDIA UNDER DIFFERENT UPSTREAM BOUNDARY CONDITIONS

Bidur Ghimire[1], Shinichiro Nakashima[2] and Takashi Hosoda[3]

[1] Ph.D. Student, Department of Urban Management, Kyoto University
C1-3, Kyodai-Katsura, Kyoto, 615-8540, Japan, e-mail: ghimireb@umdriv.mbox.media.kyoto-u.ac.jp
[2] Res. Associate, Pioneering Research Unit for Next Generation, Kyoto University
104, Inttech Center, Kyodai-Katsura, Kyoto, 615-8530, Japan, e-mail: s.nakashima@hx7.ecs.kyoto-u.ac.jp
[3] Professor, Department of Urban Management, Kyoto University
C1-3, Kyodai-Katsura, Kyoto, 615-8540, Japan, e-mail: hosoda@mbox.kudpc.kyoto-u.ac.jp

ABSTRACT

The free surface flow of an incompressible fluid through a porous medium is a physical phenomenon of great importance in many practical situations. In this paper, we deal with the unsteady lateral intrusion of water into porous media consisting of large grain size, which can be applied to simulate the storm water storage into granular road sub-base from a side drain channel, under prescribed upstream boundary conditions. The common fundamental equations for solid-liquid multiphase flows with the inertia and porous resistance terms are used as the basic model. The fundamental characteristics of the intrusion process are firstly investigated theoretically using the depth averaged equations with the inertia term and the porous resistance terms in momentum equations. It is pointed out that there are two distinct power law regimes with respect to time in the unsteady intrusion process. The theoretical results are verified by carrying out the two dimensional numerical simulation and hydraulic experiment. The analytical solutions obtained for the assumed similarity distribution of flow depth and velocity are found to be in good agreement with the numerical and experimental results. The gradual transition from early inertia-pressure (IP) to pressure-drag (PD) regime is also reproduced in the simulation.

Keywords: porous drag, similarity solution, granular sub-base, power law.

1. INTRODUCTION

The free surface flow of an incompressible fluid through a porous medium is a physical phenomenon of great importance in many practical situations. An important branch of porous media research involves the modelling of flow within the soil. The viscous, laminar incompressible flow in the porous media having small porosity is represented by Darcy equation (Beavers, G. S. and Joseph, D. D., 1967). In this paper, we deal with the unsteady lateral intrusion of water into porous media consisting of large grain size, which can be applied to simulate the storm water storage into granular road sub-base from a side drain channel, under prescribed upstream boundary conditions as shown in figure 1.

The common fundamental equations for solid-liquid multiphase flows with the inertia force term, which is generally neglected in the normal underground flows, are used as the basic model of this study because the pervious and granular road sub-base material consists of large grain size material. The fundamental characteristics of lateral intrusion process are firstly investigated theoretically using the depth averaged equations with the inertia term and the porous drag resistance terms in the momentum equation. Assuming the self-similarity distributions of depth and velocity, we derived the similarity solutions of intrusion process with the propagation of front position and the depth distribution under two boundary conditions. It is pointed out that there are distinct two power law regimes with respect to time

in the intrusion process.

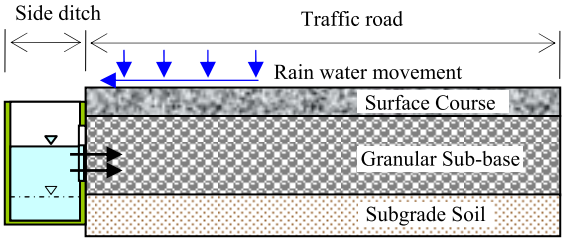

Figure 1 Schematic diagram showing the intrusion of storm water into porous sub-base from the side drain in a typical road section.

The theoretical results derived in this study are verified by carrying out the numerical simulations and a hydraulic experiment. The vertical 2-D numerical simulation is done applying the finite volume method with volume of fluid (VOF) technique. It is pointed out that the power law of propagation of front position, the distribution of depth, etc. can be reproduced in the results of simulations and hydraulic experiments.

2. FLOW DOMAIN AND BOUNDARY CONDITIONS OF INTRUSION PROCESS

Two types of flow domains are considered for the study of intrusion dynamics of fluid into the porous media. The two conditions defined in this paper as Case A and Case B (see figure 2) represent the domains subjected to constant upstream water level and constant upstream discharge boundary conditions, respectively. The front propagation speed, the velocity and the depth distribution of free surface flow in the porous media are studied where similarity solutions for each of the cases are derived as well.

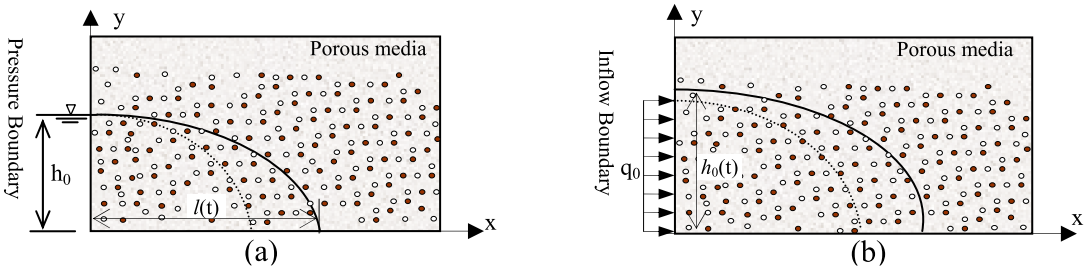

Figure 2 Schematic diagrams showing flow domains subjected to constant upstream (a) water level h_0 (Case A) and (b) inflow discharge q_0 (Case B)

3. THEORETICAL CONSIDERATIONS

The governing equations for the conservation of mass and momentum as given in the section 4 are taken as the basic equations. In order to investigate fundamental characteristics of intrusion process, the simplified depth averaged equations are used. The depth averaged continuity and momentum equations for one dimensional flow with inertia and drag resistance terms can be written as:

$$\frac{\partial\{(1-C)h\}}{\partial t}+\frac{\partial\{(1-C)hU\}}{\partial x}=0 \tag{1}$$

$$\frac{\partial\{(1-C)hU\}}{\partial t}+\frac{\partial\{(1-C)hU^2\}}{\partial x}=-(1-C)gh\frac{\partial z_s}{\partial x}+\frac{\partial}{\partial x}\left\{(1-C)\frac{\tau_{xx}}{\rho}h\right\}-\frac{\tau_{bx}}{\rho}-\frac{R_x}{\rho}h \tag{2}$$

where t is time, x the spatial coordinate, h the flow depth, U the depth averaged velocity, z_s the free surface elevation, τ_{xx} the viscous stress, τ_{bx} the bottom shear stress and ρ the density of water. For the analytical study, the volumetric concentration of solid particles C is taken

constant for the rigid porous media. The last term with R_x of eq. 2 represents the porous resistance term. Hence for the conventional laminar and non-inertial flow in porous media if we neglect the shear stress and inertia terms in eq. 2, we get the expression of the Darcy's Law in which the term R_x is defined as,

$$\frac{R_x}{\rho} = \frac{g(1-C)^2}{K}U \tag{3}$$

where K is the hydraulic conductivity of the porous medium. The resistance law for turbulent flow is also considered later, where porous resistance is assumed to be proportional to the squared power of velocity. Taking (1-C) and K to be constant and neglecting the shear stress terms in eq. 1 and eq. 2 we get the following set of continuity and momentum equation for the analytical study subjected to various boundary conditions.

$$\frac{\partial h}{\partial t} + \frac{\partial hU}{\partial x} = 0 \tag{4}$$

$$\frac{\partial U}{\partial t} + U\frac{\partial U}{\partial x} + g\frac{\partial h}{\partial x} = -C_D U \tag{5}$$

where C_D is given by C_D=g(1-C)/K.

The approximate solutions for depth and velocity distributions are derived based on the similarity of depth and velocity to clarify the fundamental characteristics of lateral intrusion of water under two boundary conditions. The method based on similarity was applied to the dam break flow of viscous fluid where temporal and spatial distribution of depth, velocity and front position were derived analytically balancing the pressure gradient and viscous terms (Herbert, E. H., 1982; Hosoda, T., Kokado, T. and Miyagawa, T., 2000).

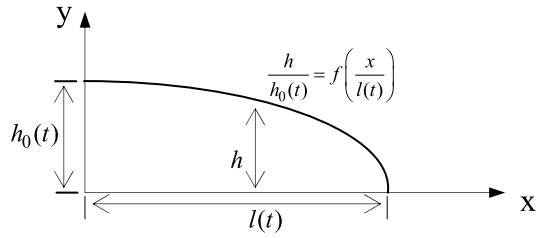

Figure 3 Definition of similarity distribution for flow depth

Figure 3 shows the similarity distribution of depth in free surface flow in terms of characteristic depth $h_0(t)$ and front length l(t). In this paper we derive the similarity solutions for different flow regimes where Inertia-Pressure terms and Pressure-Drag terms are balanced in the flow under two different boundary conditions. The distribution of inflow velocity U_0, depth at origin h_0, and the front position l are expressed in terms of temporal powers a, b and c as given by

$$U_0 = \alpha V_0\left(\frac{t}{T_0}\right)^a, \quad h_0 = \beta L_0\left(\frac{t}{T_0}\right)^b \text{ and } \quad l = \gamma L_0\left(\frac{t}{T_0}\right)^c \tag{6}$$

where α, β and γ are constant coefficients; V_0, L_0 and T_0 are the characteristic velocity , length and time respectively. These characteristic parameters are explained for each of the cases considered in its respective section. It will be shown that the power laws with respect to time given by eq. 6 are valid for the dominance of the combination of two terms of Inertia-Pressure and Pressure-Drag regimes. Also the analytical solutions based on assumed similarity distributions are derived. The similarity distributions of the depth $h(x,t)$ and velocity $U(x,t)$ are defined as

$$h = h_0 F\left(\frac{x}{l(t)}\right), \quad U = U_0 G\left(\frac{x}{l(t)}\right) \tag{7}$$

where the functions F and G are the distribution functions for depth and velocity, respectively. In the subsequent sections, we derive the temporal powers a, b and c and the expressions for flow depth h, flow velocity U and front position l.

3.1 Derivation of similarity solution for Case A

This is the condition where upstream boundary is set at a constant water depth h_0. The characteristic time, length and velocity in this case are defined as

$$T_0 = \left(h_0 / g\right)^{\frac{1}{2}}, \quad L_0 = h_0 \quad \text{and} \quad V_0 = \left(g h_0\right)^{\frac{1}{2}} \tag{8}$$

Using eq. 6 and eq. 7, the equations for continuity and momentum as expressed by eq. 4 and eq. 5 are reduced to eq. 9 and eq. 10 as below,

$$-\xi \frac{\gamma L_0}{T_0} c(t')^{c-1} \frac{dF}{d\xi} + \alpha V_0 (t')^a \frac{dGF}{d\xi} = 0 \tag{9}$$

$$\underbrace{\alpha \frac{V_0}{T_0} a t'^{a-1} G - \alpha \frac{V_0}{T_0} c t'^{a-1} \xi \frac{dG}{d\xi}}_{inertia(unsteady)} + \underbrace{\frac{\alpha^2}{\gamma} \frac{V_0^2}{L_0} t'^{2a-c} G \frac{dG}{d\xi}}_{inertia(convection)} + \underbrace{\frac{\beta}{\gamma} g t'^{b-c} \frac{dF}{d\xi}}_{pressure} = \underbrace{-C_D \alpha V_0 t'^a G}_{drag} \tag{10}$$

where t' is the non-dimensional time defined as $t' = t/T_0$ and ξ the ratio $x/l(t)$. Due to the constant water level boundary condition, h_0 is constant i.e.

$$b = 0 \tag{11}$$

And from eq. 9, we can write

$$c - a = 1 \tag{12}$$

For the determination of the values of temporal power coefficients a, b and c, each combination of eq. 10 such as Inertia-Pressure terms and Pressure-Drag terms are taken and solved for the coefficients. The results are as given below.

(i) Inertia-Pressure regime:

$$a = 0, \quad b = 0 \quad \text{and} \quad c = 1 \tag{13}$$

(ii) Pressure-Drag regime:

$$a = -1/2, \quad b = 0 \quad \text{and} \quad c = 1/2 \tag{14}$$

(iii) Inertia-Drag regime:

No solution is obtained for this regime.

The similarity solutions, for the assumed distribution of depth and velocity along with the derived powers, are found for both regimes as depicted above by the transformed continuity and momentum equations are presented below

(i) Inertia-Pressure regime

The sets of equations for this regime will then be given by

$$-\frac{\gamma L_0}{T_0} \xi \frac{dF}{d\xi} + \alpha V_0 \frac{dGF}{d\xi} = 0 \tag{15}$$

$$-\alpha \frac{V_0}{T_0} \xi \frac{dG}{d\xi} + \frac{\alpha^2}{\gamma} \frac{V_0^2}{L_0} G \frac{dG}{d\xi} + \frac{\beta}{\gamma} g \frac{dF}{d\xi} = 0 \tag{16}$$

Also the velocity of front U_F can be derived by taking the time derivative of $l(t)$ as below

$$U_F = \frac{dl}{dt} = \gamma L_0 c t'^{c-1} \frac{1}{T_0} = \frac{\gamma L_0}{T_0} \tag{17}$$

Assuming G and F as the function of ξ as below,

$$G = 1\text{-}A\xi,\ A = \text{const.} \tag{18}$$

$$F = 1\text{-}\xi \tag{19}$$

Using these values of G and F in eq. 15 and eq. 16 and after some simplification we get,

$$\alpha V_0 = \sqrt{gh_0},\quad \beta L_0 = h_0 \quad \text{and} \quad \gamma L_0 = 2T_0\sqrt{gh_0} \tag{20}$$

The velocity and depth at origin and the front position are derived as

$$U_0 = \sqrt{gh_0},\quad h_0 = h_0 \quad \text{and} \quad l = 2t\sqrt{(gh_0)} \tag{21}$$

The flow depth and velocity are then derived as

$$h = h_0 F\left(\frac{x}{l(t)}\right) = h_0\left(1 - \frac{x}{2\sqrt{gh_0}}\frac{1}{t}\right) \quad \text{and} \quad U = U_0 G\left(\frac{x}{l(t)}\right) = \left(\sqrt{gh_0}\right)\left(1 + \frac{x}{l(t)}\right) \tag{22}$$

(ii) Pressure-Drag regime

The governing equations for this regime can be written as

$$-\frac{\gamma L_0}{2T_0}\xi\frac{dF}{d\xi} + \alpha V_0 \frac{dGF}{d\xi} = 0 \tag{23}$$

$$\frac{\beta}{\gamma} g \frac{dF}{d\xi} = -C_D \alpha V_0 G \tag{24}$$

Thus using the same functional form of flow depth and velocity, eq. 23 and eq. 24 yield

$$\alpha V_0 = \frac{1}{2}\left(\frac{gh_0}{T_0 C_D}\right)^{\frac{1}{2}},\ \beta L_0 = h_0 \quad \text{and} \quad \gamma L_0 = \left(\frac{4gT_0 h_0}{C_D}\right)^{\frac{1}{2}} \tag{25}$$

Now using eq. 8 and eq. 25, velocity and depth at origin and the front positions are derived as

$$U_0 = \frac{1}{2}\left(\frac{gh_0}{C_D}\right)^{\frac{1}{2}} t^{-\frac{1}{2}},\ h_0 = h_0 \quad \text{and} \quad l = \left(\frac{4gh_0}{C_D}\right)^{\frac{1}{2}} t^{\frac{1}{2}} \tag{26}$$

Similarly the overall flow depth and velociy can be written as

$$h = h_0 F\left(\frac{x}{l(t)}\right) = h_0\left(1 - \frac{x}{l(t)}\right) \quad \text{and} \quad U = U_0 G\left(\frac{x}{l(t)}\right) = \frac{1}{2}\left(\frac{gh_0}{C_D}\right)^{\frac{1}{2}}\left(1 + \frac{x}{l(t)}\right)t^{-\frac{1}{2}} \tag{27}$$

3.2 Derivation of similarity solution for Case B

This is the condition where upstream boundary is set at a constant flux i.e. there is a constant value of inflow discharge q_0. The characteristic time, length and velocity in this case are defined as

$$T_0 = \left(\frac{q_0}{g^2}\right)^{\frac{1}{3}},\quad L_0 = \left(\frac{q_0^2}{g}\right)^{\frac{1}{3}} \quad \text{and} \quad V_0 = \left(gq_0\right)^{\frac{1}{3}} \tag{28}$$

Using eq. 6 and eq. 7, the equations for continuity and momentum as expressed by eq. 4 and eq. 5 are reduced to eq. 29 and eq. 30 as below

$$\beta\frac{L_0}{T_0}b(t')^{b-1}F-\beta\frac{L_0}{T_0}c(t')^{b-1}\xi\frac{dF}{d\xi}+\frac{q_0}{\gamma L_0}(t')^{-c}\frac{dGF}{d\xi}=0 \tag{29}$$

$$\underbrace{\alpha\frac{V_0}{T_0}at'^{a-1}G-\alpha\frac{V_0}{T_0}ct'^{a-1}\xi\frac{dG}{d\xi}}_{inertia(unsteady)}+\underbrace{\frac{\alpha^2}{\gamma}\frac{V_0^2}{L_0}t'^{2a-c}G\frac{dG}{d\xi}}_{inertia(convection)}+\underbrace{\frac{\beta}{\gamma}gt'^{b-c}\frac{dF}{d\xi}}_{pressure}=\underbrace{-C_x\alpha V_0t'^{a}G}_{drag} \tag{30}$$

The upstream constant flux boundary i.e. constant discharge condition is given by

$$U_0h_0=q_0(=const.)$$

$$\text{i.e. } \alpha\beta V_0L_0(t')^{a+b}=q_0 \tag{31}$$

With the use of eq. 28 through eq. 31, the temporal powers are obtained and are shown in table 1. Also the similarity solutions for various hydraulic variables are obtained and shown in eq. 32 and eq. 33, in which the use of powers and the assumed distribution functions are made along with transformed governing equations for the case considered.

(i) Inertia-Pressure regime

$$h=h_0F\left(\frac{x}{l(t)}\right)=\left(\frac{q_0^{\,2}}{g}\right)^{\frac{1}{3}}\left(1-\frac{x}{l(t)}\right)\ \text{ and }\ U=U_0G\left(\frac{x}{l(t)}\right)=(gq_0)^{\frac{1}{3}}\left(1+\frac{x}{l(t)}\right) \tag{32}$$

(ii) Pressure-Drag regime

$$U=U_0G\left(\frac{x}{l(t)}\right)=\left(\frac{q_0g}{2C_x}\right)^{\frac{1}{3}}\left(1+\frac{x}{3l(t)}\right)t^{-\frac{1}{3}}\ \text{ and }\ h=h_0F\left(\frac{x}{l(t)}\right)=\left(\frac{2q_0^{\,2}C_x}{g}\right)^{\frac{1}{3}}t^{\frac{1}{3}}\left(1-\frac{x}{l(t)}\right) \tag{33}$$

3.3 Power law derivation for turbulent flows

Theoretical derivation of temporal powers a, b and c for the turbulent flow in highly permeable porous media is also made here. When the Darcy law breaks owing to high velocity of flow, the linear resistance law is no longer valid (Harry, R.C. 1989). Thus the momentum sink term contributing to the pressure gradient due to porous media is assumed to be proportional to the fluid velocity squared. Hence the resistance term used in eq. 3 can be written as

$$R_x/\rho=C_TU^2 \tag{34}$$

where C_T is the coefficient used for the resistance law of turbulent flow in porous media. In this study, the effect of Reynold's number is not considered on C_T so that the coefficient C_T is assumed to be dependent only on the porous media characteristics. The temporal powers are derived for such turbulent flows in the porous media having large permeability. A summary of the theoretical results obtained for both linear and squared power resistance law for all the cases are given in table 1.

Table 1 Summary of power law derivations

Assumed power law distribution	**Resistance law**	**Case A**		**Case B**		**Explanation**
		IP	**PD**	**IP**	**PD**	
$U_0=\alpha V_0\left(\frac{t}{T_0}\right)^a$, $h_0=\beta L_0\left(\frac{t}{T_0}\right)^b$,	linear	$a=0$	$a=-1/2$	$a=0$	$a=-1/3$	U_0, h_0: velocity and depth at origin.
	power of	$b=0$	$b=0$	$b=0$	$b=1/3$	l: length of front.
	velocity	$c=1$	$c=1/2$	$c=1$	$c=2/3$	V_0, L_0 and T_0:
$l=\gamma L_0\left(\frac{t}{T_0}\right)^c$; where α, β and γ	squared	$a=0$	$a=-1/3$	$a=0$	$a=-1/4$	characteristic velocity,
	power of	$b=0$	$b=0$	$b=0$	$b=1/4$	length and time,
are constant coefficients.	velocity	$c=1$	$c=2/3$	$c=1$	$c=3/4$	respectively.

4. OUTLINE OF EXPERIMENTAL SETUP

A hydraulic experiment was carried out for the evaluation of the proposed model. A transparent perspex flume filled with glass bead was used. In the experiment glass beads of 1mm diameter was used as porous media and a constant water level of 85 mm was maintained at the left boundary so as to simulate Case A. The velocity and depth of flow with free surface were taken using digital movie camera placed near the side of the flume. The position of front and depth of flow for different time is tracked by the image interpretation with the help of graduations made on the perspex plate of the flume facing the camera. The time dependence and the flow profile of the intrusion behaviour observed during the experiment are compared with the analytical solution and numerical simulation as well.

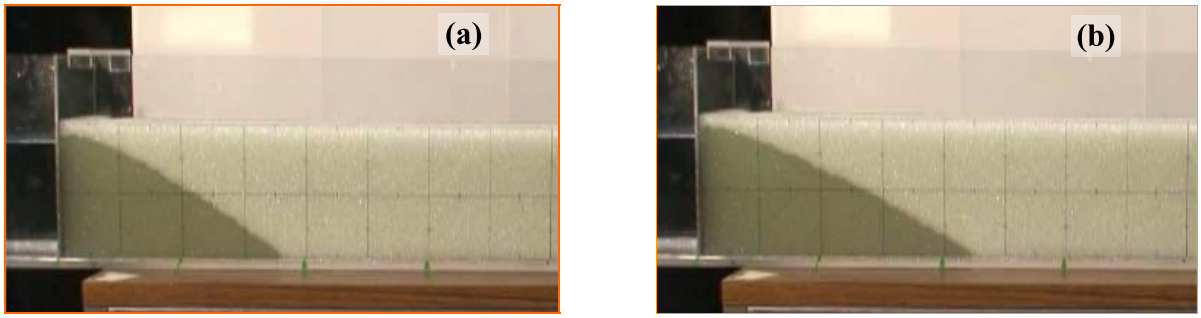

Figure 4 Flow profile during the experiment at time (a) 5s (b) 10s

The experiment was carried out until it attained a steady state condition. The permeability was also calculated using the hydraulic gradient when the system attained steady state. The measured steady state discharge and the flow depths have been used for the calculation of the value of permeability of the media. A couple of snapshots showing the spatial and temporal change of flow profile during the experiment is also given in figure 4.

5. NUMERICAL SIMULATION

5.1 Basic equations

The governing equations in vertical two-dimension for the flow in porous media are formulated below for the incompressible fluid. The equation for the phase continuity of the fluid is given by

$$\frac{\partial(1-C)}{\partial t}+\frac{\partial(1-C)u}{\partial x}+\frac{\partial(1-C)v}{\partial y}=0 \tag{35}$$

and the momentum equations in x and y directions extended with the porous media drag resistance terms can be written as

$$\frac{\partial\{(1-C)u\}}{\partial t}+\frac{\partial\{(1-C)u^2\}}{\partial x}+\frac{\partial\{(1-C)uv\}}{\partial y} = -(1-C)\frac{1}{\rho}\frac{\partial p}{\partial x}+\nu\left(\frac{\partial^2(1-C)u}{\partial x^2}+\frac{\partial^2(1-C)u}{\partial y^2}\right)-\frac{R_x}{\rho}+(1-C)g_x \tag{36}$$

and

$$\frac{\partial\{(1-C)v\}}{\partial t}+\frac{\partial\{(1-C)uv\}}{\partial x}+\frac{\partial\{(1-C)v^2\}}{\partial y} = -(1-C)\frac{1}{\rho}\frac{\partial p}{\partial y}+\nu\left(\frac{\partial^2(1-C)v}{\partial x^2}+\frac{\partial^2(1-C)v}{\partial y^2}\right)-\frac{R_y}{\rho}+(1-C)g_y \tag{37}$$

where, $R_x=\rho g(1\text{-}C)^2u/K$ and $R_y=\rho g(1\text{-}C)^2v/K$. In above equations u and v are the velocity components of fluid in x and y directions respectively; ρ is fluid density and ν the kinematic viscosity. K and C are the hydraulic conductivity and solid phase concentration of the media so the term $(1\text{-}C)$ represents the porosity of the media. The Darcy's velocity and the pore space velocity are related as

$$\mathbf{U} = (1-C)\mathbf{V} \tag{38}$$

where, **U** is Darcy's velocity or Darcy's flux and **V** is the pore velocity vector (u,v). The hydraulic conductivity for laminar flow in porous media can be found by Kozeny-Carman formula in which K is given by

$$K = \frac{g\varepsilon^3 d^2}{180\nu(1-\varepsilon)^2} \tag{39}$$

where ε and d are the porosity and particle diameter respectively.

A number of numerical calculations are made for different values of hydraulic parameters and the boundary conditions as well which are listed in Table 2.

Table 2 List of Numerical Run

Numerical Run	Case	Parameters
RUN1	A	K=0.250m/s, C=0.6, h_0 =0.050m
RUN2	A	K=0.010m/s, C=0.6, h_0 =0.085m
RUN3	B	K=0.005m/s, C=0.5, U_0=0.01m/s
RUN4	B	K=0.010m/s, C=0.6, U_0=0.05m/s

5.2 Numerical methods

The governing flow equations 35 to 37 are solved by finite volume method in a staggered computational grid where velocities are defined at the cell faces and all other scalar variables are at the cell centre. The pressure is iteratively adjusted using Highly Simplified Marker and Cell (HSMAC) method (Hirt, C.W. and Cook, J.L., 1972). The velocity changes induced by each pressure change are added to the velocities computed before, enforcing thereby to satisfy the continuity equation. The free surface kinematics is traced using VOF technique (Hirt, C.W. and Nichols, B.D., 1981). For the flow in porous domain the time evolution of the fraction of fluid function $(1\text{-}C)F$ is governed by the following relation

$$\frac{\partial(1-C)F}{\partial t} + \frac{\partial u(1-C)F}{\partial x} + \frac{\partial v(1-C)F}{\partial y} = 0 \tag{40}$$

where $(1\text{-}C)F$ represents the portion of cell occupied by the fluid i.e. cell saturation (Jacimovic et al., 2005).

6. RESULTS AND DISCUSSIONS

The theoretical results are verified using the results of simulations. The velocity profiles obtained by numerical runs are shown in Figures 5 and 6 for Case A and Case B, respectively. The result of numerical simulation for Case B also shows that there is an increase in the depth near the origin in the Pressure-Drag regime as depicted by the theory with a temporal power 1/3. Figure 7 shows front position vs. time for both cases. Thus the results of the numerical runs presented here clearly show the existence of distinct two regimes: Inertia-Pressure and Pressure-Drag for both cases. The results are in close agreement with the analytical solution derived with similarity assumption. All the results presented here correspond to the linear resistance law. The value of permeability for the numerical simulation of the experiment has been calculated by Kozeny-Carman formula and it was compared with the values obtained from both the experiment and analytical formula as obtained in eq. 26.

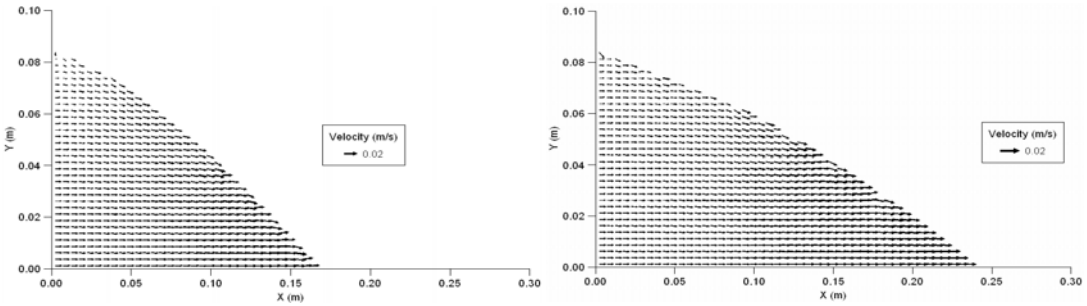

(a) (b)

Figure 5 Velocity profiles for Case A (RUN2) at time (a) 5s and (b) 10s

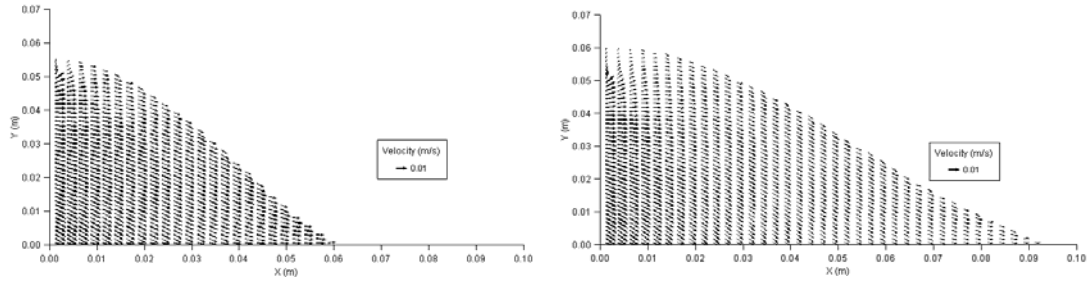

(a) (b)

Figure 6 Velocity Profiles for Case B at time (a) 5s and (b) 10s (RUN3)

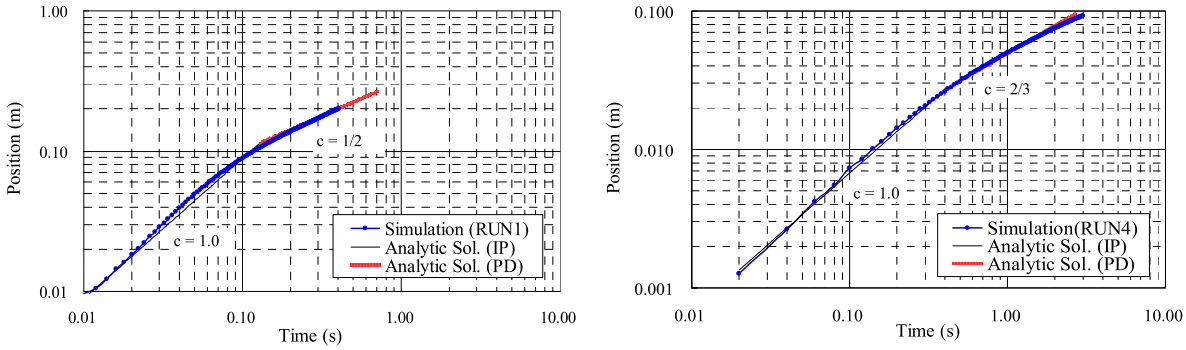

(a) (b)

Figure 7 Temporal position of front (a) Case A: $K = 0.25 ms^{-1}$, $h_0 = 0.05m$ (b) Case B: $K = 0.01 ms^{-1}$, $U_0 = 0.05\ ms^{-1}$,$q_0 = 0.0025 m3/s$ per m)

The flow profiles are reproduced in the numerical run (RUN2) which is in close agreement with that of the experiment (Figure 8). The experimental depths are slightly greater than that of the analytical and numerically simulated values. The reason may be due to the continuous rise of capillary fringe which was also observed in the experiment. Figure 9 in the next page shows the comparison among the experimental, numerical and analytic results. We can point out the dominance of the Pressure-Drag regime for low permeable media as expectected.

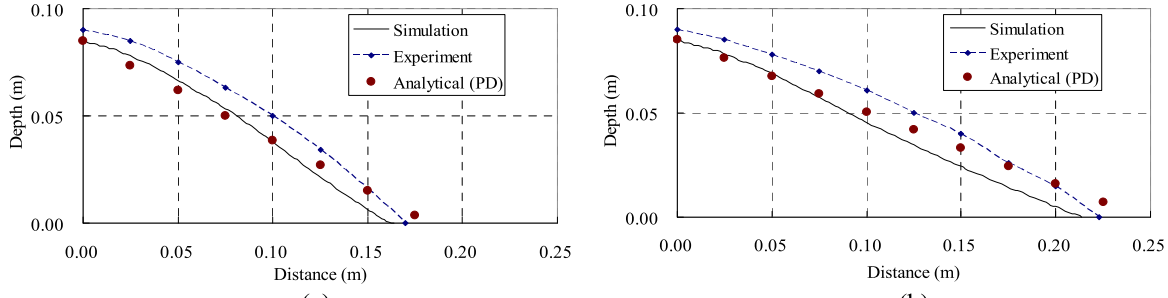

(a) (b)

Figure 8 Flow Profiles for Case A at time (a) 5s and (b) 10s

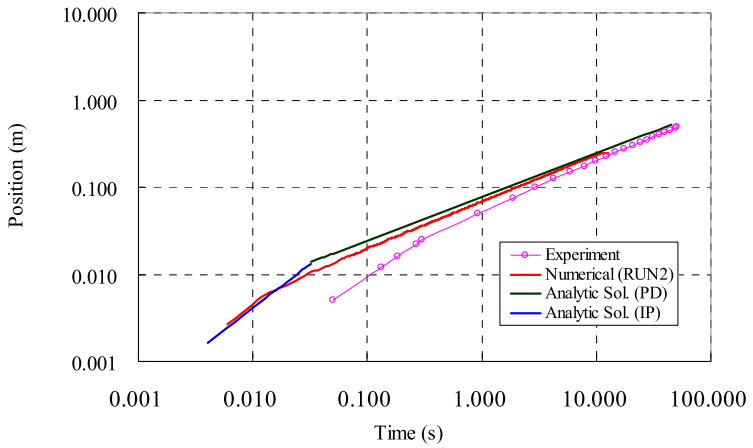

Figure 9 Temporal position of front under constant upstream water level (Case A)

7. CONCLUSIONS

In this paper, the lateral unsteady intrusion processes of water into porous media under two boundary conditions are studied using inertia term and porous resistance term in the equation of motion. If we assume similarity distributions of depth and velocity and the dominance of the two terms of inertia-pressure and pressure-drag, the temporal power solutions for characteristic depth, length and velocity can be derived for inertia-pressure(IP) regime and pressure-drag(PD) regime respectively under two boundary conditions. The similarity solutions are also derived analytically. The vertical 2D numerical simulations of porous media flows were carried out using VOF method. The numerical results showed that IP regime appeared first with the higher temporal power followed by PD regime with lower temporal power. The dominance of PD regime was observed in the hydraulic experiment with the glass beads of diameter 1mm. The spatial and temporal distribution of the depth profile of simulation is in good agreement with the experiments.

This research will be continued to make clear the regime of the turbulent flow where non-darcy effect should be taken into account with the non-dimensional parameter C_T . Further experiments with large size glass beads will be carried out to verify the existence of clear inertial- pressure regime.

REFERENCES

Beavers, G. S. and Joseph, D. D. (1967), Boundary conditions at the natural permeable wall, *J. Fluid Mech*., 30, pp.197–207.

Huppert, H. E. (1982), The propagation of two-dimensional and axisymmetric viscous gravity currents over a rigid horizontal surface, *J. Fluid Mech.*, 121, pp.43–58.

Hosoda, T., Kokado, T. and Miyagawa, T. (2000), Flow characteristics of viscous fluids on the basis of self-similarity law and its applications to high flow concrete., *J. of Applied Mech.,* JSCE, 3, pp.313-321.

Harry, R. C. (1989), Seepage, Drainage, and flow nets, John Wiley & Sons, Newyork.

Hirt, C.W. and Cook, J.L. (1972), Calculating Three Dimensional Flows around structures and over Rough Terrain, *J. Comput. Phys*., 10, pp.324-340.

Hirt, C.W. and Nichols, B.D. (1981), Volume of fluid (VOF) method for the dynamics of free boundaries, *J. Comput. Phys*., 39, pp.201-225.

Jacimovic, N., Hosoda, T., Kishida, K. and Ivetic, M. (2005), Numerical Solution of the Navier-Stokes equations for incompressible flow in porous media with free surface boundary, *J. of Applied Mech.,* JSCE, 8, pp.225-231.